Hindawi
Mathematical Problems in Engineering
Volume 2017, Article ID 4965262, 13 pages
https://doi.org/10.1155/2017/4965262

Research Article

Optimizing Shrinkage Curves and Application in Image Denoising

Hongyao Deng,[1,2] Qingxin Zhu,[1] Jinsong Tao,[3] and Xiuli Song[4]

[1] *School of Information & Software Engineering, University of Electronic Science and Technology of China, Chengdu 611731, China*
[2] *College of Computer Engineering, Yangtze Normal University, Chongqing 408000, China*
[3] *School of Electrical Engineering, Wuhan University, Wuhan 430072, China*
[4] *School of Computer Science and Technology, Chongqing University of Posts and Telecommunications, Chongqing 400065, China*

Correspondence should be addressed to Hongyao Deng; hydeng_2004@163.com

Received 9 November 2016; Revised 9 March 2017; Accepted 14 March 2017; Published 30 April 2017

Academic Editor: Bogdan Dumitrescu

Copyright © 2017 Hongyao Deng et al. This is an open access article distributed under the Creative Commons Attribution License, which permits unrestricted use, distribution, and reproduction in any medium, provided the original work is properly cited.

A shrinkage curve optimization is proposed for weighted nuclear norm minimization and is adapted to image denoising. The proposed optimization method employs a penalty function utilizing the difference between a latent matrix and its observation and uses odd polynomials to shrink the singular values of the observation matrix. As a result, the coefficients of polynomial characterize the shrinkage operator fully. Furthermore, the Frobenius norm of the penalty function is converted into the corresponding spectral norm, and thus the parameter optimization problem can be easily solved by using off-and-shelf plain least-squares. In the practical application, the proposed denoising method does not work on the whole image at once, but rather a series of matrix termed Rank-Ordered Similar Matrix (ROSM). Simulation results on 256 noisy images demonstrate the effectiveness of the proposed algorithms.

1. Introduction

Low rank matrix approximation has been attracting significant research interest in recent years. This approach aims to reconstruct the latent data from its degraded observation matrix and is frequently applied in many fields, such as machine learning [1], computer version [2], recommendation system [3], and image processing [4]. As a branch of this research, a regularized nuclear norm minimization problem is widely considered over matrices,

$$\min_{\mathbf{X}\in\mathbb{R}^{n\times m}} \left(f(\mathbf{X}) + \mu \|\mathbf{X}\|_* \right), \tag{1}$$

where $\mathbf{X}$ denotes a matrix, scalar $\mu > 0$ is a parameter, and $f(\mathbf{X})$ and $\|\mathbf{X}\|_*$ are the data fidelity term and the data regularization term, respectively. In this formula, $\|\mathbf{X}\|_* = \sum_{i=1}^{\min(m,n)} \sigma_i(\mathbf{X})$ is called the nuclear norm of $\mathbf{X}$, where $\sigma_i(\mathbf{X})$ denotes the ith largest singular value of $\mathbf{X}$.

If $f(\mathbf{X})$ is convex, then $f(\mathbf{X}) + \mu\|\mathbf{X}\|_*$ is a convex function because nuclear norm $\|\mathbf{X}\|_*$ is also convex. Thus, problem (1) is a convex optimization problem and can be treated by using various classic iterative optimization algorithms including steepest-descent, conjugate-gradient, and interior-point algorithms. When the data fidelity term $f(\mathbf{X}) = 1/2\|\mathbf{X}-\mathbf{Y}\|_F^2$, where $\mathbf{Y}$ is an observation matrix and $\|\cdot\|_F$ denotes the Frobenius norm operator, this is the well-known nuclear norm minimization (NNM) [5]. The NNM problem was proved that it can be solved by applying a soft threshold operation on the singular values of $\mathbf{Y}$, and the solution can be achieved using a Singular Value Thresholding (SVT) algorithm [6].

Despite the success of NNM, it is not flexible enough to handle more complex issues. To pursue the convex property, NNM treats each singular value equally. As a result, the soft-thresholding operator shrinks each singular value by the same amount [6]. In principal component analysis however, different principal directions quantify different information. For example, the large singular value delivers the major feature information such as edges and texture. This implies that, in image denoising, the larger the singular value is, the lesser the amount shrinks. Obviously, the NNM model and the corresponding solver cannot handle this issue.

To overcome this limitation, a regularized nuclear norm minimization with weights was put forward. These weights may enhance the representation capability of the original nuclear norm. Its form is as follows:

$$\min_{\mathbf{X}\in\mathbb{R}^{n\times m}}\left(f(\mathbf{X})+\sum_{i=1}^{\min(m,n)} g[i]\,\sigma_i(\mathbf{X})\right), \quad (2)$$

where $g[i]$ is the weight designed to $\sigma_i(\mathbf{X})$.

Problem (2) is a nonconvex nonsmooth low rank minimization problem. Of course, if $g[i]$ is replaced with μ, problem (2) reverts to problem (1). Solving problem (2) is challenging, or even NP-hard. To solve this problem, researchers presented some assumption to handle it. Gu et al. [7] assumed that g is nondescending on $[0,\infty)$, $0 \le g[1] \le \cdots \le g[\min(m,n)]$, and thus problem (2) becomes convex and can be solved by a soft-thresholding operation. Moreover, the authors devised a solver in which $g[i]$ is inversely proportional to $\sigma_i(\mathbf{X})$. Gasso et al. [8] argued that if both f and $-g$ are convex, problem (2) can be solved by DC (Difference of Convex functions) programming. Lu et al. [9] assumed that g is concave increasing monotonically on $[0,\infty)$ and f satisfies Lipschitz continuous condition; the weights are achieved at the super gradient point of the concave function g. Based on this assumption, the authors proposed Iteratively Reweighted Nuclear Norm (IRNN) method. In addition, Hu et al. [10] reported their Truncated Nuclear Norm Regularization (TNNR) method, based on the same assumptions as in [9].

By applying these low rank matrix approximation theories, different image denoising methods have been reported. For example, a method of coupling sparse denoising and unmixing with low rank constraint is proposed for hyperspectral image in [11]; a scheme of incorporating iterative support detection into TNNR is presented to reduce white Gaussian noise in [12]; the eigenvectors of the Laplacian are considered to suppress Gaussian noise in [13]; a weighted nuclear norm minimization model is presented [14] and is used in three applications, that is, image denoising, background subtraction, and image completion. These methods achieve high quality results. A main reason is that all of them employ a powerful patch-based technique.

Inspired by weighted nuclear norm minimization and patch-based technique, a parameter optimization method is proposed in this paper. The proposed method utilizes the difference between a latent matrix and its observation to design a penalty function and employs odd polynomials to shrink the singular values of the observation matrix. As a result, the coefficients of polynomial fully characterize the shrinkage operator. Furthermore, for the penalty function, its Frobenius norm is converted into a spectral norm. Thereby, the parameter optimization can be easily solved by using plain least-squares.

To validate the effectiveness, the optimization theory is applied in image denoising. Since the proposed method is to optimize shrinkage curves, it is called OSC method. In the practical application, the OSC method does not work on the whole image at once, but rather a series of matrix termed Rank-Ordered Similar Matrix (ROSM, see Definition 2). Thirty-two images were tested. Experimental results show that the OSC method achieves better results than the Bilateral Filter; when the noisy standard deviation is less than 20, the results achieved by OSC are better than those by BM3D, and when the noisy standard deviation varies from 20 to 40, the results by OSC are weaker than by BM3D.

The contribution of this paper is twofold. Firstly, in the penalty function devised for weighted nuclear norm minimization, the weight representation is replaced by odd polynomials. So, the coefficients of polynomial characterize the role of the weights fully. Furthermore, the Frobenius norm of the penalty function is converted into a spectral norm. Secondly, the proposed optimization method is adapted to image denoising. Experimental results show that the proposed OSC method outperforms the Bilateral Filter and also is superior to the BM3D method on the case of low noise.

The rest of paper is organized as follows. In Section 2, the shrinkage curve optimization is formulated. Section 3 describes the image denoising algorithm, and the corresponding analysis is followed in Section 4. Section 5 reports the experimental results, and conclusions are drawn in Section 6.

2. Optimizing Shrinkage Curves

In this section, the problem to be discussed is formulated, and the method of optimizing shrinkage curves is followed.

2.1. Problem Formulation. Let $\mathbf{X}$ be a unknown square matrix in $\mathbb{R}^{n\times n}$, and let $\mathbf{Y}$ be its observation. The observed matrix is corrupted by white Gaussian noise $\mathbf{N}$ with deviation σ^2. This is expressed as

$$\mathbf{Y}=\mathbf{X}+\mathbf{N}. \quad (3)$$

To reconstruct the original square matrix $\mathbf{X}$ from its noisy version, the following weighted nuclear norm minimization with a constraint is considered:

$$\begin{aligned} \min \quad & \|\mathbf{X}\|_{*,\mathbf{w}}, \\ \text{subject to} \quad & \|\mathbf{Y}-\mathbf{X}\|_F^2 < \varepsilon, \end{aligned} \quad (4)$$

where ε is a threshold, $\|\mathbf{X}\|_{*,\mathbf{w}} = \sum_i |w_i\sigma_i(\mathbf{X})|_1$, and $\|\mathbf{Y}-\mathbf{X}\|_F^2 = \sum_i\sum_j (y_{ij}-x_{ij})^2$. In this formula, $\sigma_i(\mathbf{X})$ denotes the ith largest singular value of $\mathbf{X}$, and $\|\mathbf{X}\|_{*,\mathbf{w}}$ and $\|\mathbf{Y}-\mathbf{X}\|_F$ are the weighted nuclear norm of $\mathbf{X}$ and the Frobenius norm of $(\mathbf{Y}-\mathbf{X})$, respectively. Our aim is to use polynomial coefficients to characterize the weights and obtain the solution of the problem.

2.2. Optimization Method. As in [7], it is proven that the weighted nuclear norm minimization (4) can be solved by imposing a soft threshold operation on the singular values of observation matrix. The form is as follows:

$$\mathbf{X}=\mathbf{U}S(\boldsymbol{\Sigma})\,\mathbf{V}^T, \quad (5)$$

where $\mathbf{Y} = \mathbf{U}\boldsymbol{\Sigma}\mathbf{V}^T$ is the Singular Value Decomposition (SVD) of $\mathbf{Y}$ and S is the soft-thresholding operator. This operator with weight vector $\mathbf{w}$ shrinks the singular values;

$S(\Sigma)_{ii} = \max(\Sigma_{ii} - w_i, 0)$. To obtain the thresholds, the following penalty function is employed:

$$f(S) = \left\| \mathbf{X} - \mathbf{U}S(\boldsymbol{\Sigma})\mathbf{V}^T \right\|_F^2. \tag{6}$$

Assuming that shrinkage operation is applied differently to every singular value in matrix $\boldsymbol{\Sigma}$, and thus it can be broken into

$$S(\Sigma) = \begin{bmatrix} s_1(\Sigma[1]) & 0 & \cdots & 0 \\ 0 & s_2(\Sigma[2]) & \cdots & 0 \\ \vdots & \vdots & \ddots & \vdots \\ 0 & 0 & \cdots & s_n(\Sigma[n]) \end{bmatrix}, \tag{7}$$

where $\Sigma[i]$ is the ith largest singular value of $\mathbf{Y}$ and S_i denotes the ith shrinkage operator. In our work, odd polynomials are taken to represent these shrinkage operators, where the coefficients of polynomial characterize the shrinkage operator fully. Thus, the shrinkage operator is expressed as

$$s_i(\Sigma) = \sum_{j=1}^{J} c_i[j]\,\Sigma^{2\times j-1}, \quad \text{for } i = 1, 2, \ldots, n. \tag{8}$$

Substituting (8) into (7), the shrinkage operator can be rewritten as

$$S_{\mathbf{c}}(\Sigma) = \begin{bmatrix} \sum_{j=1}^{J} c_1[j]\,\Sigma[1]^{2\times j-1} & 0 & \cdots & 0 \\ 0 & \sum_{j=1}^{J} c_2[j]\,\Sigma[2]^{2\times j-1} & \cdots & 0 \\ \vdots & \vdots & \ddots & \vdots \\ 0 & 0 & \cdots & \sum_{j=1}^{J} c_n[j]\,\Sigma[n]^{2\times j-1} \end{bmatrix}. \tag{9}$$

Substituting (9) into (6) and considering $\mathbf{V}$ is a unitary matrix, the penalty function can be rewritten as

$$f(c_1, c_2, \ldots, c_n) = \left\| \mathbf{XV} - \mathbf{U}S_{\mathbf{c}}(\Sigma) \right\|_F^2. \tag{10}$$

The focus now shifts to optimization of the penalty function. To obtain the optimal solution by using plain least-squares, the Frobenius norm in (10) is converted into a spectral norm. For ease of formulation, a vector $\mathbf{c} \in \mathbb{R}^{nJ}$ is defined that contains all the coefficients series: $\{c_i[j] : j = 1, \ldots, J\}$, for $i = 1, 2, \ldots, n$; that is,

$$\mathbf{c}^T = [c_1[1], c_1[2], \ldots, c_1[J], c_2[1], \ldots, c_n[1], c_n[2], \ldots, c_n[J]]. \tag{11}$$

A matrix $\mathbf{Z} \in \mathbb{R}^{n^2 \times nJ}$ is also defined that is a block-diagonal matrix with n blocks,

$$\mathbf{Z} = \begin{bmatrix} \mathbf{z}[1] & & & \\ & \mathbf{z}[2] & & \\ & & \ddots & \\ & & & \mathbf{z}[n] \end{bmatrix}, \tag{12}$$

where each of the blocks $\mathbf{z}[i]$ is size of $n \times J$, with the content

$$\mathbf{z}[i] = \begin{bmatrix} 1 \\ 1 \\ \vdots \\ 1 \end{bmatrix} * \left[\Sigma[i]^1 \;\; \Sigma[i]^3 \;\; \cdots \;\; \Sigma[i]^{2\times J-1} \right], \quad \text{for } i = 1, 2, \ldots, n. \tag{13}$$

In addition, two operators, vec and diag, are introduced. The vec operator returns a vector by concatenating the columns in a matrix; the diag operator returns a diagonal matrix by putting the elements of a vector on the main diagonal. For example, if $\mathbf{M} = [m_{11}, m_{12}; m_{21}, m_{22}]$ is a matrix, vec $(\mathbf{M})$ returns the vector $\mathbf{m} = (m_{11}, m_{21}, m_{12}, m_{22})^T$; if $\mathbf{m} = (m_1, m_2, m_3, m_4)^T$ is a vector, diag $(\mathbf{m})$ returns the diagonal matrix where the main diagonal is (m_1, m_2, m_3, m_4).

Using these notations and operators, the penalty function (10) can be rewritten as

$$\begin{aligned} f(\mathbf{c}) &= \left\| \operatorname{vec}(\mathbf{XV}) - \operatorname{diag}(\operatorname{vec}(\mathbf{U}))\,\mathbf{Zc} \right\|_2^2 \\ &= \left\| \mathbf{b} - \mathbf{AZc} \right\|_2^2, \end{aligned} \tag{14}$$

where $\mathbf{b} = \operatorname{vec}(\mathbf{XV})$ and $\mathbf{A} = \operatorname{diag}(\operatorname{vec}(\mathbf{U}))$.

The optimal set of parameters that define the shrinkage curves is

$$\frac{\partial f(\mathbf{c})}{\partial \mathbf{c}} = 0 = \mathbf{AZ}^T(\mathbf{AZc} - \mathbf{b}), \tag{15}$$

which leads to

$$\mathbf{c}_{\text{opt}} = \left[\mathbf{Z}^T\mathbf{A}^T\mathbf{A}\mathbf{Z}\right]^{-1}\left[\mathbf{Z}^T\mathbf{A}^T\mathbf{b}\right]. \tag{16}$$

3. Application in Image Denoising

In this section, the OSC method is introduced for image denoising, containing denoising modeling data and the denoising algorithm.

3.1. Denoising Modeling Data. The proposed OSC method does not work on the whole image at once, but rather a matrix-set in which each matrix contains a fixed number of similar patches extracted from the original noisy images. A patch is first defined as follows.

Definition 1. $\mathbf{Y}$ denotes an image, sized $N_1 \times N_2$ pixels. Let $y_r = \mathbf{Y}(i, j)$ be a reference pixel. A block of size $\sqrt{n} \times \sqrt{n}$ is extracted from $\mathbf{Y}$, where y_r resides at the top-left corner. By applying vec to the block, the $\sqrt{n}\times\sqrt{n}$ block is identified with a vector in $\mathbb{R}^n$. The corresponding patch is defined by

$$\begin{aligned}\mathbf{p}_r &= \operatorname{vec}\begin{pmatrix} \mathbf{Y}(i, j) & \cdots & \mathbf{Y}(i, j+\sqrt{n}-1) \\ \vdots & \ddots & \vdots \\ \mathbf{Y}(i+\sqrt{n}-1, j) & \cdots & \mathbf{Y}(i+\sqrt{n}-1, j+\sqrt{n}-1) \end{pmatrix} \\ &= \begin{pmatrix} y_r \\ \vdots \\ y_{r+n-1} \end{pmatrix},\end{aligned} \tag{17}$$

where $i \in \{1, 2, \ldots, N_1 - \sqrt{n}+1\}$ and $j \in \{1, 2, \ldots, N_2 - \sqrt{n}+1\}$. When all pixels are complete, a patch-set in $\mathbb{R}^n$ can be built, denoted by $\mathscr{P} = \{\mathbf{p}_r : r = 1, 2, \ldots, (N_1 - \sqrt{n}+1) \times (N_2 - \sqrt{n}+1)\}$.

Definition 2. Let $\mathbf{p}_r \in \mathscr{P}$ be a reference patch and $\|\cdot\|$ denote the Euclidean norm; the distance between $\mathbf{p}_r$ and $\mathbf{p}_j$ can be calculated, using the metric

$$d_{rj} = \left\|\mathbf{p}_r - \mathbf{p}_j\right\|_2, \quad \text{for } \mathbf{p}_j \in \mathscr{P}. \tag{18}$$

These scalar distances are then sorted and the patches in $\mathscr{P}$ are correspondingly ordered,

$$\begin{aligned} d_{r(1)} \le d_{r(2)} \le \cdots \le d_{r(M)} &\longrightarrow \mathbf{p}_{(1)} \prec \mathbf{p}_{(2)} \prec \cdots \\ &\prec \mathbf{p}_{(M)}, \end{aligned} \tag{19}$$

where $d_{r(j)}$ denotes the jth smallest distance value, $\prec$ denotes the order relation between patches, and $M = |\mathscr{P}| = (N_1 - \sqrt{n}+1) \times (N_2 - \sqrt{n}+1)$ denotes the number of patches in $\mathscr{P}$. The denoising modeling data, termed Rank-Ordered Similar Matrix (ROSM), are defined as

$$\mathbf{Y}_r = \operatorname{ROSM}(r) = \left(\mathbf{p}_{(1)}, \mathbf{p}_{(2)}, \ldots, \mathbf{p}_{(n)}\right). \tag{20}$$

Obviously, ROSM is a square matrix of size $n\times n$ and $\mathbf{p}_{(1)} = \mathbf{p}_r$. When all patches in $\mathscr{P}$ are complete, a matrix-set in $\mathbb{R}^{n\times n}$ can be built, denoted by $\widetilde{\mathscr{M}} = \{\mathbf{Y}_r : r = 1, 2, \ldots, M\}$.

3.2. Denoising Algorithm. The proposed denoising algorithm consists of Algorithms 1 and 2. The former trains the polynomial coefficients $\mathbf{c}_{\text{opt}}$, and the latter reduces noise.

Suppose $\mathbf{Y}$ is a noisy image and $\mathbf{X}$ is its noise-free version. Based on Definition 2, the matrix-set $\widetilde{\mathscr{M}}$ of $\mathbf{Y}$ is built, and the corresponding noise-free matrix-set is also obtained, denoted by $\mathscr{M} = \{\mathbf{X}_r : r = 1, \ldots, M\}$. Thereby, there exist M paired samples $\{(\mathbf{X}_r, \mathbf{Y}_r) : r = 1, \ldots, M\}$ to train $\mathbf{c}_{\text{opt}}$. The corresponding penalty function is as follows:

$$f(\mathbf{c}) = \sum_{r=1}^{M} \left\|\mathbf{X}_r\mathbf{V}_r - \mathbf{U}_r S_{\mathbf{c}}(\boldsymbol{\Sigma}_r)\right\|_F^2, \tag{21}$$

where $\mathbf{U}_r\boldsymbol{\Sigma}_r V_r^T$=SVD$(\mathbf{Y}_r)$. The optimum parameters are

$$\mathbf{c}_{\text{opt}} = \left[\sum_{r=1}^{M}\left(\mathbf{Z}_r^T\mathbf{A}_r^T\mathbf{A}_r\mathbf{Z}_r\right)\right]^{-1}\left[\sum_{r=1}^{M}\left(\mathbf{Z}_r^T\mathbf{A}_r^T\mathbf{b}_r\right)\right], \tag{22}$$

where $\mathbf{b}_r = \operatorname{vec}(\mathbf{X}_r\mathbf{V}_r)$, $\mathbf{A}_r = \operatorname{diag}(\operatorname{vec}(\mathbf{U}_r))$, and $\mathbf{Z}_r$ can be obtained by using (12) and (13).

Next, the two-iteration denoising algorithm is introduced. Suppose $\mathbf{Y}$ is a noisy image to be processed, of size $N_1 \times N_2$. Employing Definition 2, the matrix-set $\widetilde{\mathscr{M}}$ of $\mathbf{Y}$ is built. For any ROSM $\mathbf{Y}_r$ in $\widetilde{\mathscr{M}}$, the estimate of its noise-free version can be obtained by

$$\widehat{\mathbf{X}}_r = \mathbf{U}_r S_{\mathbf{c}}(\boldsymbol{\Sigma}_r)\mathbf{V}_r^T, \tag{23}$$

where $\mathbf{Y}_r = \mathbf{U}_r\boldsymbol{\Sigma}_r\mathbf{V}_r^{\mathrm{T}}$ is the SVD of $\mathbf{Y}_r$ and $S_{\mathbf{c}}(\boldsymbol{\Sigma}_k)$ is expressed as (10). When all ROSMs in $\widetilde{\mathscr{M}}$ are complete, an estimated-set can be built, denoted by $\widehat{\mathscr{M}} = \{\widehat{\mathbf{X}}_r : r = 1, 2, \ldots, M\}$. Every estimate $\widehat{\mathbf{X}}_r$ is put back into the original image canvas, then intensities of pixels falling in the same position in the canvas are averaged. And thus, the first-estimate of the noise-free image is obtained, denoted by $\widehat{\mathbf{X}}(t = 1)$. Repeating the above operations again, the second-estimate $\widehat{\mathbf{X}}(t = 2)$ is also yielded.

In addition, a scaled version of the residual error, the difference between the noisy and estimated image, is considered. Let R_r denote the operation putting the rth estimate $\widehat{\mathbf{X}}_r$ back into the original image canvas; the denoising method can be expressed as the following tuples formula:

$$\begin{aligned} \widehat{\mathbf{X}}(t) &= \left(\sum_{r=1}^{M} R_r\left(\mathbf{U}_r S_{\mathbf{c}(t)}(\Sigma_r)\mathbf{V}_r^T\right)\right) \oslash \mathbf{D} \\ \widehat{\mathbf{Y}}(t) &= \widehat{\mathbf{X}}(t) + \gamma\left(\mathbf{Y} - \widehat{\mathbf{X}}(t)\right), \\ &\qquad\qquad \text{for } t = 1, 2, \end{aligned} \tag{24}$$

where $\widehat{\mathbf{X}}(t)$ is the tth image estimate, $\widehat{\mathbf{Y}}(t)$ is the tth adjustment, γ is the scaled factor of residual error, $\oslash$ denotes entry-wise division, and $\mathbf{D}$ denotes the matrix with the same size as the noisy image, in which each entry records the number that the pixel on the same location is processed.

```
Input: $N$ paired images, $\{(\mathbf{X}(i), \mathbf{Y}(i)) \mid i = 1, 2, \ldots, N\}$
    Initialize the table $\mathbf{W} = \mathbf{0}$;
    for $t = 1 : 2$
        Initialize a parameter $c_{\text{opt}}(t) = [\mathbf{0}]$;    // of size $nJ \times 1$.
        for $i = 1 : N$
            Initialize $\mathbf{S}_1 = [\mathbf{0}]$;
            Initialize $\mathbf{s}_2 = [\mathbf{0}]$;
            Get a paired images, $(\mathbf{X}, \mathbf{Y}) \leftarrow (\mathbf{X}(i), \mathbf{Y}(i))$;
            Based on Definition 1, extract all patches from image $\mathbf{Y}$ and build the patch-set $\mathscr{P} = \{\mathbf{p}_r\}$
            for each patch $\mathbf{p}_r$ in $\mathscr{P}$ do
                Based on Definition 2, obtain a ROSM $\mathbf{Y}_r$;
                Obtain the matrix $\mathbf{X}_r$ corresponding to $\mathbf{Y}_r$;
                Singular value decomposition, $[\mathbf{U}_r \mathbf{\Sigma}_r \mathbf{V}_r^T] = \text{SVD}(\mathbf{Y}_r)$;
                Map $\mathbf{X}_r \mathbf{V}_r$ to a vector, $\mathbf{b}_r = \text{vec}(\mathbf{X}_r \mathbf{V}_r)$;
                Map $\mathbf{U}_r$ to a diagonal matrix, $\mathbf{A}_r = \text{diag}(\text{vec}(\mathbf{U}_r))$;
                Map $\mathbf{\Sigma}_r$ to a diagonal block matrix $\mathbf{Z}_r$, according to Eq. (12) and (13);
                Accumulation, $\mathbf{S}_1 = \mathbf{S}_1 + \mathbf{Z}_r^T \mathbf{A}_r^T \mathbf{A}_r \mathbf{Z}_r$;
                Accumulation, $\mathbf{s}_2 = \mathbf{s}_2 + \mathbf{Z}_r^T \mathbf{A}_r^T \mathbf{b}_r$;
            end for
            Obtain a optimized parameter, $c_{\text{opt}}(t) = [\mathbf{S}_1]^{-1}[\mathbf{s}_2]$;
            if $t = 1$ do
                for each patch $\mathbf{p}_r$ in $\mathbf{Y}$ do
                    Obtain the estimation $\widehat{\mathbf{Y}}_r = \mathbf{U}_r S_{\mathbf{c}}(\mathbf{\Sigma}_r)\mathbf{V}_r^T$;
                    Plug $\widehat{\mathbf{Y}}_r$ into the image canvas of the noisy image $\mathbf{Y}$;
                end for
                Obtain a new $\mathbf{Y}(i) \leftarrow$ Average the pixels for fixed position in the image canvas;
            end if
            Save the $\mathbf{c}_{\text{opt}}(t)$ to Table $\mathbf{W}$;
        end for
    end for
Output: Table $\mathbf{W}$ that containing the parameters $\mathbf{c}_{\text{opt}}$.
```

Algorithm 1: Training the coefficients $\mathbf{c}_{\text{opt}}$.

```
Input: Noisy image $\mathbf{Y}$ and the shrinkage parameters $\mathbf{c}(t)$
    Initialize the intermediate image $\widehat{\mathbf{X}}(0) = (\mathbf{Y} - \mathbf{127})/\mathbf{128}$ and adjusted image $\widehat{\mathbf{Y}}(0) = (\mathbf{Y} - \mathbf{127})/\mathbf{128}$;
    MIN = mix $((\mathbf{Y} - \mathbf{127})/\mathbf{128})$;
    MAN = max $((\mathbf{Y} - \mathbf{127})/\mathbf{128})$;
    for $t = 1 : 3$
        Set a counter to zeros, $\mathbf{D} = [\mathbf{0}]$;
        Obtain an adjusted estimate, $\widehat{\mathbf{Y}}(t) = \widehat{\mathbf{X}}(t-1) + \gamma(\mathbf{Y} - \widehat{\mathbf{X}}(t-1))$;
        According to Definition 1, build the patch-set $\mathscr{P} = \{p_r\}$, associated with image $\mathbf{Y}$;
        for each patch $p_r$ in $\mathscr{P}$ do
            According to Definition 2, obtain a ROSM $\mathbf{Y}_r$;
            Singular value decomposition, $[\mathbf{U}_r \mathbf{\Sigma}_r \mathbf{V}_r^T] = \text{SVD}(\mathbf{Y}_r)$;
            Find the parameter $\mathbf{c}(t)$ corresponding to $\mathbf{Y}_r$ from Table $\mathbf{W}$;
            Obtain the estimation $\widehat{\mathbf{Y}}_r = \mathbf{U}_r S_{\mathbf{c}}(\mathbf{\Sigma}_r)\mathbf{V}_r^T$;
            if $(\widehat{\mathbf{Y}}_r < \text{MIN})$, then $\widehat{\mathbf{Y}}_r = \mathbf{Y}_r$;
            if $(\widehat{\mathbf{Y}}_r > \text{MAN})$, then $\widehat{\mathbf{Y}}_r = \mathbf{Y}_r$;
            Put $\widehat{\mathbf{Y}}_r$ back into the image canvas;
            In counter $\mathbf{D}$, the entries associated with pixels in $\widehat{\mathbf{Y}}_r$ is added by 1;
        end for
        Obtain an estimated image, $\widehat{\mathbf{X}}(t) \leftarrow$ obtained canvas image is entry-wisely divided by $\mathbf{D}$;
    end for
Output: The final estimated image $\widehat{\mathbf{Y}}(3) \times \mathbf{128} + \mathbf{127}$.
```

Algorithm 2: Optimizing shrinkage curves based denoising algorithm.

4. Algorithm Analysis

In this section, the influence of different levels of noise for the singular vectors is first discussed; then the shrunken scales of singular values are analyzed.

4.1. Influence of Different Levels of Noise for Singular Vectors. Two matrices, $\mathbf{Y}_\alpha$ and $\mathbf{Y}_\beta$, are chosen arbitrarily from the noisy matrix-set $\widetilde{\mathscr{M}}$, and $\mathbf{y}(\alpha) = \operatorname{vec}(\mathbf{Y}_\alpha)$ and $\mathbf{y}(\beta) = \operatorname{vec}(\mathbf{Y}_\beta)$. Thus, $\mathbf{y}(\alpha) = \mathbf{x}(\alpha) + \mathbf{n}(\alpha)$ and $\mathbf{y}(\beta) = \mathbf{x}(\beta) + \mathbf{n}(\beta)$, where $\mathbf{x}$ denotes the noise-free vector and $\mathbf{n}$ is white noise. The squared Euclidean distance between the two vectors $\mathbf{y}(\alpha)$ and $\mathbf{y}(\beta)$ is

$$\begin{aligned}\|\mathbf{y}(\alpha)-\mathbf{y}(\beta)\|_2^2 = \|\mathbf{x}(\alpha)-\mathbf{x}(\beta)\|_2^2 \\ + 2\langle \mathbf{x}(\alpha)-\mathbf{x}(\beta), \mathbf{n}(\alpha)-\mathbf{n}(\beta)\rangle \\ + \|\mathbf{n}(\alpha)-\mathbf{n}(\beta)\|_2^2,\end{aligned} \quad (25)$$

where the symbol $\langle\cdot\rangle$ is the inner-product operator.

The vector difference, $\mathbf{n}(\alpha)-\mathbf{n}(\beta)$, is the Gaussian noise with covariance matrix $2\sigma^2 n^2\mathbf{I}$, where symbol $\mathbf{I}$ denotes identity matrix. Based on the argument in [15], if the dimension of $\mathbf{y}$ is large, the norm squared, $\|\mathbf{n}(\alpha)-\mathbf{n}(\beta)\|_2^2$, is concentrated around its mean $2\sigma^2 n^2$, with high probability. Similarly, the projection $\langle \mathbf{x}(\alpha)-\mathbf{x}(\beta), \mathbf{n}(\alpha)-\mathbf{n}(\beta)\rangle$ of the noise on the deterministic vector $\mathbf{x}(\alpha)-\mathbf{x}(\beta)$ is concentrated around 0 with high probability. Therefore, (17) can be interpreted as a translation-invariant procedure.

On the other hand, as the noise level increases, the singular vectors of $\mathbf{Y}_r \in \widetilde{\mathscr{M}}$ are no longer aligned with the original singular vectors of noise-free matrix $\mathbf{X}_r$. As a result, the number of reliable singular vectors of $\mathbf{Y}_r$ becomes smaller. For example, when $\mathbf{X}_r$ is corrupted by Gaussian noise at very small magnitude, all the singular vectors of $\mathbf{Y}_r$ track the noise; when corrupted at a large magnitude, the number of the singular vectors tracking the noise becomes smaller. Therefore, at increasing noise level, the singular vectors of $\mathbf{Y}_r$ become more and more unreliable and result in worse restored feature.

4.2. Shrunken Scales of Different Singular Values. Let $(\mathbf{Y}_r, \mathbf{X}_r)$ be a paired samples and $\mathbf{\Sigma}[i]$ be the ith largest singular value of $\mathbf{Y}_r \in \mathbb{R}^{n\times n}$. The coefficients vector $\mathbf{c}_{\text{opt}}$, of size $nJ\times 1$, is trained on the paired samples and then is divided into n parts; $(c_i)^T = [c_i[1], c_i[2], \ldots, c_i[J]]$ for $i = 1, 2, \ldots, n$, where c_i corresponds to the ith largest singular value of $\mathbf{Y}_r$. And thus, the estimate of the ith largest singular value of $\mathbf{Y}_r$ is as follows:

$$\widehat{\Sigma}[i] = \sum_{j=1}^{J} c_i[j](\Sigma[i])^{2*j-1}, \quad \text{for } i = 1, 2, \ldots, n. \quad (26)$$

To observe the shrunken scales of the different $\mathbf{\Sigma}[i]$ visually, the shrinkage curves are shown in Figure 1. Test results show that (i) different singular values $\mathbf{\Sigma}[i]$ have different shrunk scales; (ii) the larger the singular value, the smaller the shrunk scales; (iii) the shrunken scales for fixed index singular value are almost the same although $\mathbf{Y}_r$ is corrupted by different levels of noise.

5. Experiments

In this section, the OSC denoising performance is evaluated. In Section 5.1, setting parameters are formulated. Section 5.2 introduces two metrics, the Peak Signal-to-Noise-Ratio (PSNR) and the Mean Structural Similarity Index Measure (MSSIM). Section 5.3 reports the experimental results, and the comparisons with other methods are discussed.

5.1. Setting Parameters. A total of three parameters are set in the proposed method, a scale factor γ of residual error, an integer J regulating odd polynomial order, and a patch-size $\sqrt{n}\times\sqrt{n}$. The large γ may lead to oscillatory effects. For all noise levels, it is desirable for γ to be set to 0.1. To study the effect of parameters $(J, \sqrt{n})$ on denoising, the coefficients vector $\mathbf{c}_{\text{opt}}$ was trained on the Lena image, and the trained $\mathbf{c}_{\text{opt}}$ is used to reduce noise for the Barbara image. The influences of J and $\sqrt{n}$ for PSNR results are shown in the left and right insets in Figure 2, respectively. By experience, these parameter values used in our experiments are shown in Table 1. During implementation process, because the behavior of coefficients $\mathbf{c}_{\text{opt}}$ on large entries may be completely distorted, thereby an input value outside the training range may be violently magnified. For this case, the algorithm checks whether the input is within the learning data range, and if not, it is not modified at all.

5.2. Two Metrics. The PSNR measurement is based on pixel intensity errors between the noise-free and the restored images, given in decibels (dB). Higher PSNR means better denoising capability. Let $\mathbf{X}$ and $\widehat{\mathbf{X}}$ be the noise-free and the restored image, respectively, $|\mathbf{X}|$ denote the cardinality of $\mathbf{X}$, and $\|\cdot\|_F$ denote the Frobenius norm; the calculation of PSNR is as follows:

$$\text{PSNR} = 20\log_{10}\left(\frac{255}{|\mathbf{X}|^{-1}\sum_{q=1}^{3}\left\|\mathbf{X}^q - \widehat{\mathbf{X}}^q\right\|_F^2}\right). \quad (27)$$

The MSSIM measurement is the mean SSIM that yields mean value of structural similarities. MSSIM values are bounded in the range $[0, 1]$, and the closer the value is to 1, the better the denoising scheme is implied. The calculation of SSIM involves paired blocks extracted from the noise-free image $\mathbf{X}$ and the restored $\widehat{\mathbf{X}}$, respectively. Let y_1 and y_2 denote paired blocks, μ_{y_1} and μ_{y_2} be the mean values of y_1 and y_2, respectively, σ_{y_1} and σ_{y_2} be respective variances, and $\sigma_{y_1 y_2}$ be their covariance. Assuming c_1 and c_2 are two stabilization variables, the SSIM value can be calculated by

$$\text{SSIM}(y_1, y_2) = \frac{\left(2\mu_{y_1}\mu_{y_2} + c_1\right)\left(2\sigma_{y_1 y_2} + c_2\right)}{\left(\mu_{y_1}^2 + \mu_{y_2}^2 + c_1\right)\left(\sigma_{y_1}^2 + \sigma_{y_2}^2 + c_2\right)}. \quad (28)$$

5.3. Experimental Results and Comparisons. A test set was built to evaluate the OSC method, which was a combination of two groups, denoted by $\Gamma = \{\Gamma_1, \Gamma_2\}$. Each group Γ_k contained noisy images, with eight different levels of white noise. The Γ_1 group is associated with the sixteen noise-free images widely used, shown in Figure 3; the Γ_2 group

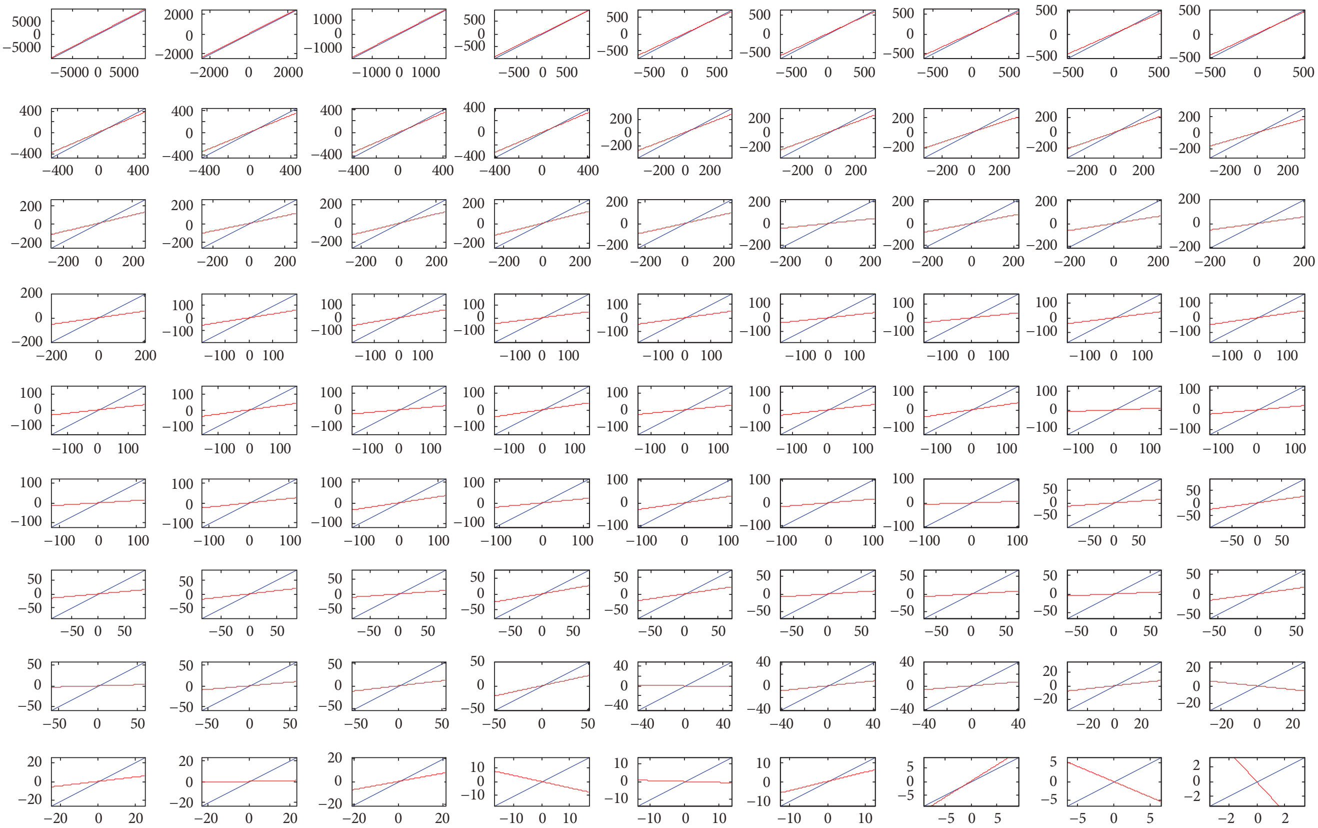

Figure 1: Illustration of the shrinkage scale of the ith largest singular value. From left to right and top to bottom, the ith inset is associated with the ith largest singular value. In each inset, the blue diagonal line is the ground singular value, and red line is its estimate. The parameters: patch-size $\sqrt{n} \times \sqrt{n} = 9 \times 9$ and $J = 1$.

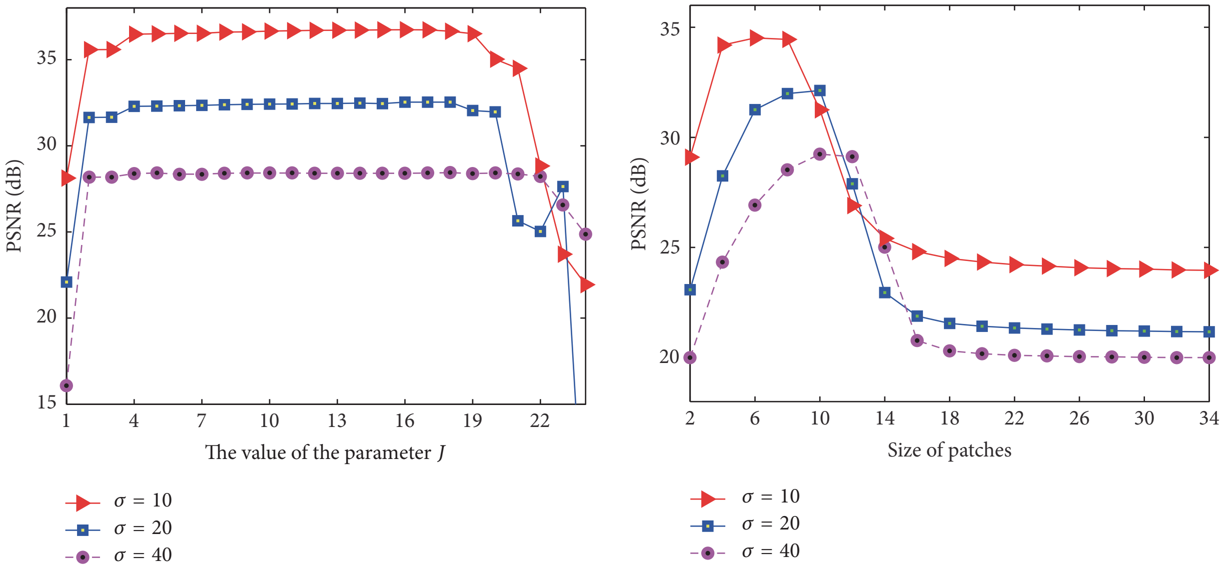

Figure 2: Illustration of influence of different parameters for denoising performance. The left inset illustrates the dependence of the parameter J on PSNR results when the size of patches is fixed to $7 * 7$. The right inset illustrates the dependence of the patch sizes on PSNR results when the parameter J is fixed to 4.

Table 1: Parameters used in training and denoising procedures.

σ	5		10		15		20		25		30		35		40	
t	1	2	1	2	1	2	1	2	1	2	1	2	1	2	1	2
γ	0.1	0.1	0.1	0.1	0.1	0.1	0.1	0.1	0.1	0.1	0.1	0.1	0.1	0.1	0.1	0.1
J	4	4	4	4	4	4	4	4	4	4	4	4	4	4	4	4
$\sqrt{n}$	6	5	7	6	8	6	9	6	10	7	11	7	12	8	12	9

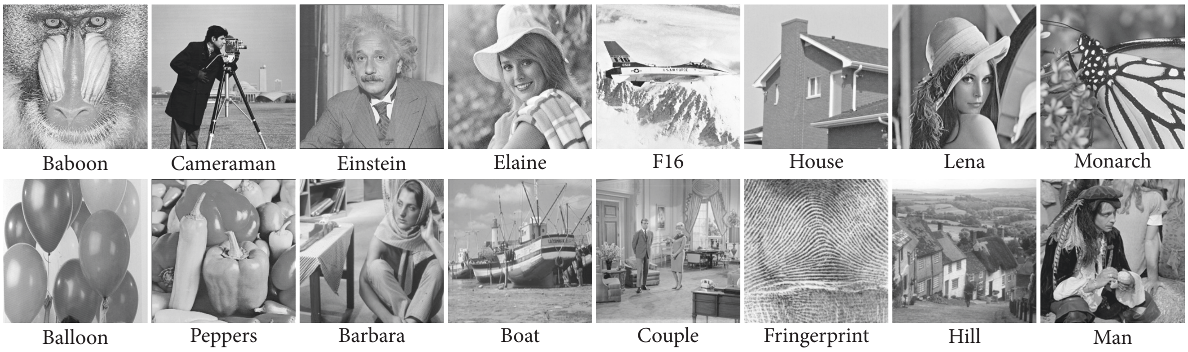

Figure 3: Sixteen widely used noise-free images associated with the group Γ_1.

is associated with the sixteen noise-free biomedical images, shown in Figure 5. These noise-free images were taken from the CVG-Granada database.

The corresponding training set was also built, which was a subset of the test Γ, denoted by $\Psi = \{\Psi_1, \Psi_2\}$. The group Ψ_1 contained the noisy versions of the five noise-free images, the Einstein, Elaine, Barbara, Fingerprint, and the Man image; the group Ψ_2 included the noisy versions of the six noise-free images, the C05c, Celulas, Cromo2, Mr2, Mr032, and the Mr034 image. The OSC method was applied to the test set Γ. Using the parameter values shown in Algorithm 1, the coefficients $\mathbf{c}_{\text{opt}}$ were trained by Algorithm 1. Algorithm 2 used the same parameter values and the trained $\mathbf{c}_{\text{opt}}$. The PSNR and MSSIM results associated with both groups are reported in Tables 2 and 3, respectively. Moreover, the visual results and zoom-in for three widely used images are shown in Figure 4 and are shown in Figure 6 for three biomedical images.

To augment the performance evaluations, the OSC method was compared with Bilateral Filter [16] and BM3D [17]. For the Bilateral Filter there are three parameters needed to be set, containing a sliding window of size $d \times d$, a geometric spread standard deviation σ_d, and a photometric spread standard deviation σ_r. The three parameters, d, σ_d, and σ_r, were set to 5, 5, and 0.1, respectively. The source codes of BM3D were taken from the original authors, and the parameter values used in the experiments were those recommended by the authors. The PSNR and MSSIM results from the two methods are reported in Table 2, and the visual results for three images are shown in Figure 4.

In addition, the mean PSNR and mean MSSIM results for fixed noise are calculated for noisy images, the Bilateral Filter, BM3D, and the OSC method, respectively. The corresponding calculations are as follows:

$$\overline{\text{PSNR}}_\sigma = \frac{1}{|\Gamma_\sigma|}\sum_{k\in\Gamma_\sigma}\text{PSNR}_\sigma(k),$$
$$\overline{\text{MSSIM}}_\sigma = \frac{1}{|\Gamma_\sigma|}\sum_{k\in\Gamma_\sigma}\text{MSSIM}_\sigma(k). \tag{29}$$

In these two formulae, Γ_σ denotes all the images with the same level noise σ in the test set Γ, and thus $|\Gamma_\sigma| = 32$; and $\text{PSNR}_\sigma(k)$ and $\text{MSSIM}_\sigma(k)$ denote the PSNR and MSSIM values of the kth image with the noise σ, respectively. For example, if the OSC method employs formula (29) to calculate, $\overline{\text{PSNR}}_5$ denotes the arithmetical mean PSNR for all images with the noise $\sigma = 5$, associated with the OSC method. The mean PSNR and MSSIM values for fixed noise for the four methods are plotted in Figure 7.

Some observations and conclusions can be drawn from the quantitative measurements and visual results. Firstly, the OSC method achieved the desirable results. The OSC method achieved the same results as the BM3D method on average and significantly outperformed the noisy method and the Bilateral Filter by 8.49 dB and 5.26 dB on average, respectively, in the PSNR results. The OSC method achieved the same results as the BM3D method on average and significantly outperformed the noisy method and the Bilateral Filter by 0.417 and 0.275 on average, respectively, in the MSSIM results. Secondly, the OSC method has a strong capability to preserve detail. The OSC method reconstructed more image details from noisy images than the Bilateral Filter and was almost the same as the BM3D.

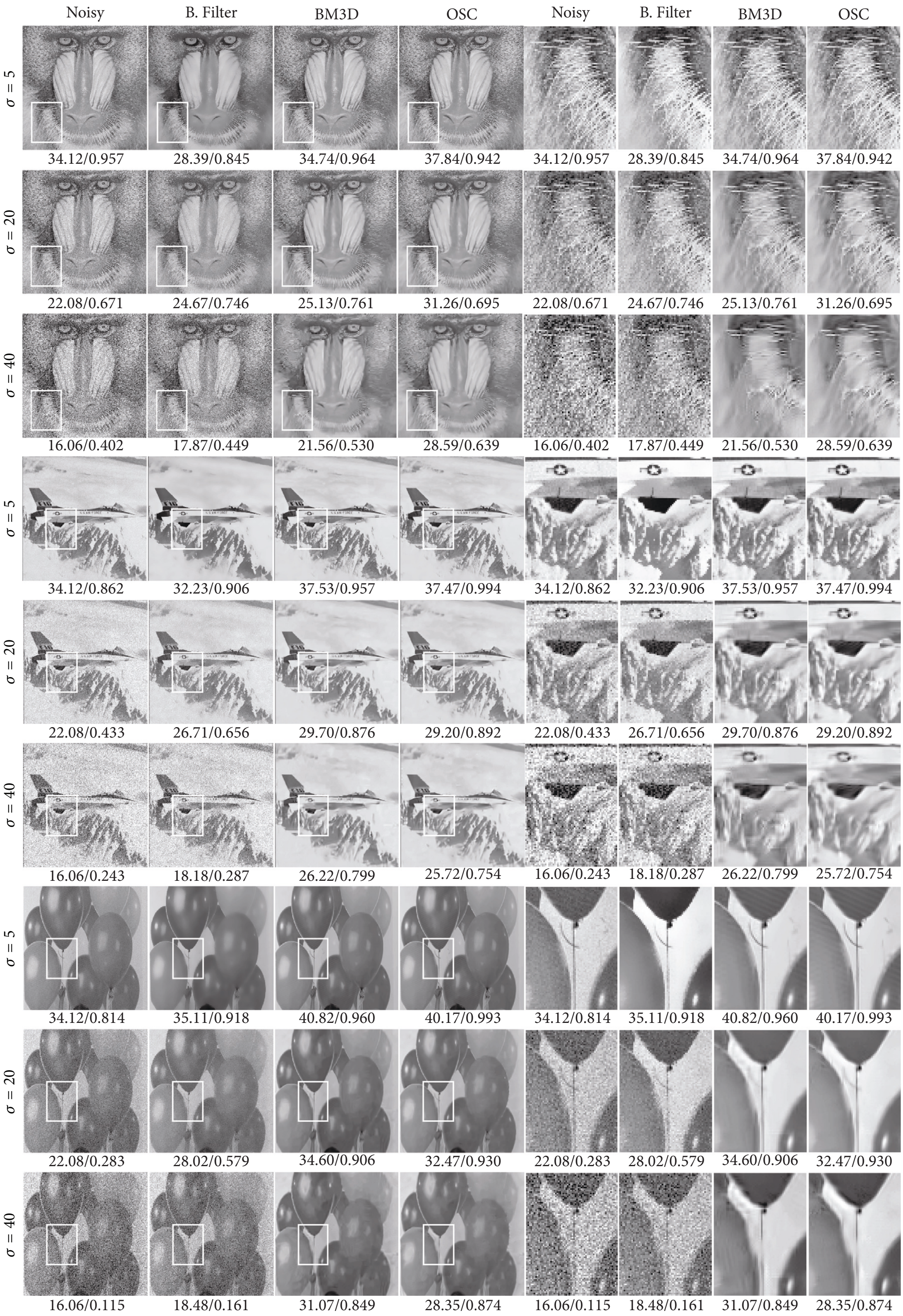

FIGURE 4: Visual results comparison. Rows are associated with denoised images and columns correspond to methods, where Columns 1–4 are the visual results and Columns 5–8 are their respective zoom-in.

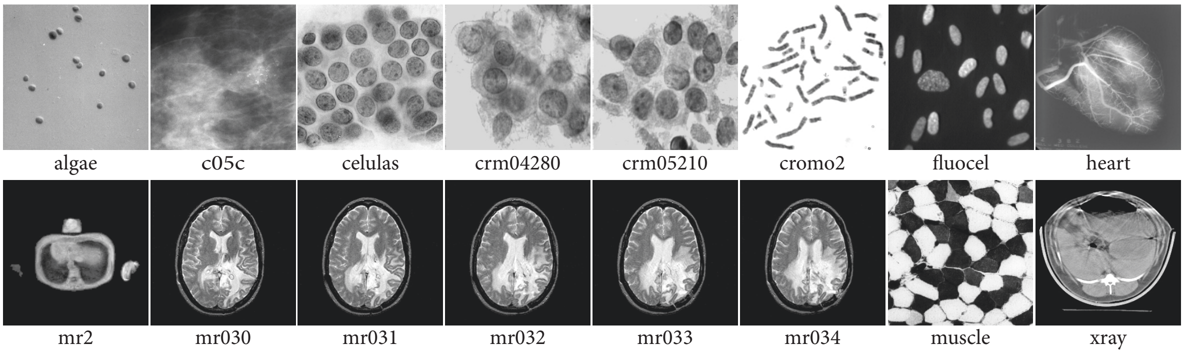

Figure 5: Sixteen noise-free biomedical images associated with the group Γ_2.

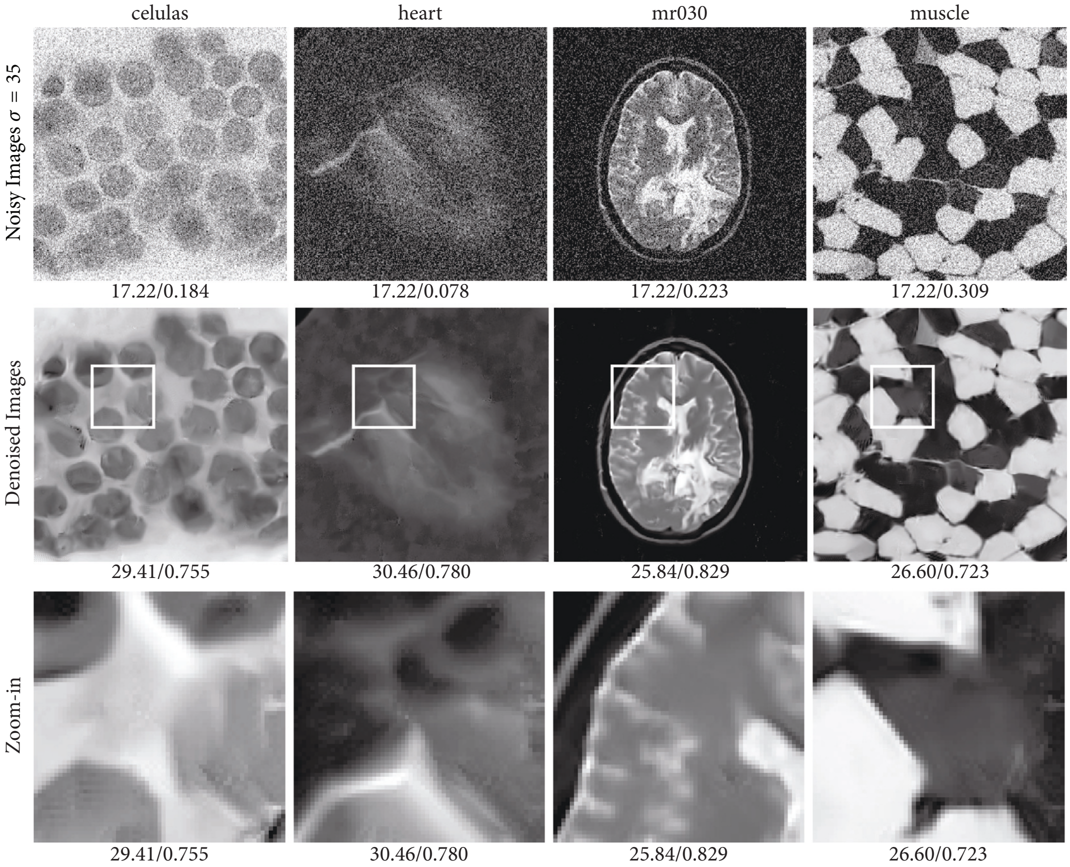

Figure 6: Visual results for four biomedical images. Row 1 corresponds to noisy images corrupted by noise ($\sigma = 35$). Row 2 corresponds to denoised images. Row 3 corresponds to zoomed-in views. Columns correspond to different images.

As seen in Figure 4, the fine-details of the moustache for the Baboon image were preserved, while the Bilateral Filter introduced excessive smoothing and resulted in visual feature blurring. Thirdly, in contrast to BM3D, the OSC method achieved decreasing results at increasing levels noise, as in Figure 7.

6. Conclusions

In this paper, a shrinkage curves optimization is proposed for weighted nuclear norm minimization. Based on the theory [7] that the weighted nuclear norm minimization can be solved by imposing a soft threshold operation on the singular values, the proposed optimization method designs a penalty function using the difference between a latent matrix and its observation and employs odd polynomials to shrink the singular values of the observation matrix. As a result, the coefficients of polynomial fully characterize the shrinkage operator. Furthermore, the Frobenius norm of the penalty function is converted into the corresponding spectral norm, so the parameter optimization can be easily solved by off-and-shelf plain least-squares.

Table 2: PSNR/SSIM comparisons with bilateral filter and BM3D.

Methods	Noise levels σ							
	5	10	15	20	25	30	35	40
(1) Baboon 256 × 256								
B. Filter	28.39/0.845	27.71/0.842	26.43/0.811	24.67/0.746	22.77/0.665	20.96/0.585	19.32/0.512	17.87/0.449
BM3D	34.74/0.964	29.62/0.899	26.91/0.830	25.13/0.761	23.84/0.693	22.89/0.633	22.16/0.580	21.56/0.530
OSC	37.84/0.942	33.95/0.846	32.49/0.762	31.26/0.695	30.41/0.650	29.72/0.627	29.09/0.621	28.59/0.639
(2) Cameraman 256 × 256								
B. Filter	32.16/0.895	31.63/0.887	29.87/0.800	27.15/0.636	24.37/0.488	21.96/0.385	19.95/0.315	18.27/0.266
BM3D	38.29/0.962	34.18/0.932	31.91/0.901	30.48/0.875	29.45/0.854	28.64/0.837	27.93/0.822	27.18/0.806
OSC	37.02/0.963	31.94/0.892	29.72/0.831	27.88/0.785	26.62/0.748	25.59/0.720	24.81/0.690	24.16/0.654
(3) Einstein 256 × 256								
B. Filter	31.48/0.802	31.19/0.804	29.73/0.739	27.17/0.598	24.45/0.452	22.05/0.340	20.04/0.261	18.36/0.206
BM3D	37.49/0.934	34.19/0.871	32.55/0.832	31.43/0.803	30.56/0.778	29.84/0.757	29.10/0.736	28.43/0.717
OSC	37.71/0.981	33.51/0.935	31.78/0.890	30.35/0.846	29.39/0.814	28.62/0.776	28.02/0.747	27.57/0.710
(4) Elaine 256 × 256								
B. Filter	31.16/0.825	30.63/0.822	29.05/0.767	26.63/0.651	24.10/0.522	21.83/0.412	19.90/0.330	18.26/0.268
BM3D	36.32/0.940	32.60/0.858	31.03/0.810	30.05/0.782	29.30/0.761	28.69/0.743	28.10/0.726	27.51/0.710
OSC	37.32/0.991	32.77/0.952	30.70/0.910	29.05/0.867	27.83/0.820	26.96/0.781	26.32/0.750	25.71/0.715
(5) F16 256 × 256								
B. Filter	32.23/0.906	31.39/0.894	29.42/0.810	26.71/0.656	24.05/0.513	21.74/0.411	19.81/0.339	18.18/0.287
BM3D	37.53/0.957	33.43/0.926	31.19/0.899	29.70/0.876	28.57/0.855	27.70/0.836	26.96/0.818	26.22/0.799
OSC	37.47/0.994	32.90/0.962	30.79/0.924	29.20/0.892	27.98/0.858	27.07/0.823	26.37/0.793	25.72/0.754
(6) Lena 256 × 256								
B. Filter	31.98/0.893	31.03/0.878	29.06/0.800	26.48/0.661	23.93/0.526	21.68/0.421	19.78/0.345	18.17/0.288
BM3D	38.16/0.961	34.49/0.932	32.40/0.906	30.95/0.883	29.86/0.863	28.99/0.844	28.23/0.825	27.43/0.805
OSC	37.06/1.000	32.14/0.973	29.83/0.939	28.05/0.906	26.84/0.878	25.89/0.861	25.13/0.840	24.49/0.798
(7) Monarch 256 × 256								
B. Filter	31.53/0.929	30.69/0.911	28.85/0.837	26.33/0.710	23.79/0.584	21.55/0.486	19.66/0.412	18.06/0.355
BM3D	38.21/0.975	34.12/0.956	31.86/0.936	30.35/0.918	29.25/0.900	28.36/0.882	27.58/0.865	26.72/0.845
OSC	37.06/0.998	31.97/0.997	29.60/0.980	27.69/0.961	26.29/0.939	25.21/0.916	24.33/0.890	23.65/0.859
(8) House 256 × 256								
B. Filter	33.76/0.878	32.88/0.870	30.59/0.777	27.51/0.602	24.58/0.442	22.10/0.331	20.06/0.259	18.37/0.210
BM3D	39.83/0.957	36.71/0.922	34.94/0.891	33.77/0.873	32.86/0.859	32.09/0.848	31.38/0.837	30.65/0.826
OSC	39.04/0.950	35.25/0.868	33.44/0.790	31.87/0.713	30.78/0.660	29.95/0.619	29.27/0.585	28.67/0.555
(9) Balloon 256 × 256								
B. Filter	35.11/0.918	34.12/0.897	31.46/0.780	28.02/0.579	24.90/0.402	22.32/0.283	20.21/0.209	18.48/0.160
BM3D	40.82/0.960	37.84/0.937	36.03/0.922	34.60/0.906	33.48/0.892	32.57/0.877	31.77/0.862	31.07/0.849
OSC	40.17/0.993	36.31/0.975	34.28/0.953	32.47/0.930	31.04/0.911	29.91/0.885	29.04/0.870	28.35/0.874
(10) Peppers 256 × 256								
B. Filter	32.68/0.907	31.67/0.889	29.51/0.803	26.72/0.654	24.04/0.510	21.74/0.402	19.80/0.325	18.18/0.269
BM3D	38.12/0.956	34.68/0.928	32.70/0.907	31.29/0.887	30.16/0.868	29.28/0.850	28.52/0.834	27.70/0.816
OSC	37.43/0.970	32.81/0.904	30.74/0.838	29.05/0.786	27.84/0.734	26.91/0.700	26.19/0.664	25.57/0.625
(11) Barbara 512 × 512								
B. Filter	31.28/0.886	30.29/0.872	28.47/0.799	26.12/0.667	23.75/0.537	21.62/0.436	19.78/0.361	18.20/0.304
BM3D	38.31/0.965	34.98/0.942	33.11/0.923	31.78/0.905	30.72/0.887	29.81/0.869	28.98/0.848	27.99/0.823
OSC	39.82/0.954	35.87/0.893	34.00/0.847	32.43/0.814	31.34/0.792	30.53/0.772	29.90/0.743	29.42/0.727
(12) Boat 512 × 512								
B. Filter	31.06/0.819	30.61/0.820	29.11/0.759	26.72/0.629	24.18/0.494	21.90/0.388	19.97/0.311	18.32/0.255
BM3D	37.28/0.939	33.92/0.888	32.14/0.854	30.88/0.826	29.91/0.801	29.12/0.780	28.43/0.759	27.74/0.739
OSC	37.74/0.996	33.19/0.967	31.08/0.939	29.36/0.904	28.11/0.876	27.17/0.857	26.40/0.840	25.79/0.826

Table 2: Continued.

Methods	Noise levels σ							
	5	10	15	20	25	30	35	40
				(13) Couple 512 × 512				
B. Filter	30.67/0.825	30.16/0.823	28.70/0.763	26.44/0.641	24.02/0.512	21.81/0.408	19.91/0.330	18.29/0.272
BM3D	37.52/0.951	34.04/0.909	32.11/0.877	30.76/0.848	29.72/0.820	28.87/0.795	28.15/0.771	27.48/0.747
OSC	38.07/0.991	33.71/0.952	31.81/0.912	30.23/0.877	29.10/0.848	28.28/0.813	27.62/0.770	27.12/0.739
				(14) Fingerprint 512 × 512				
B. Filter	29.07/0.926	27.75/0.908	25.95/0.872	24.01/0.816	22.13/0.748	20.43/0.675	18.91/0.604	17.56/0.539
BM3D	36.51/0.988	32.46/0.969	30.28/0.949	28.81/0.930	27.70/0.911	26.83/0.894	26.09/0.877	25.30/0.858
OSC	38.05/0.998	33.27/0.998	31.00/0.989	29.16/0.974	27.83/0.961	26.79/0.943	25.95/0.928	25.26/0.912
				(15) Hill 512 × 512				
B. Filter	31.03/0.804	30.66/0.804	29.27/0.745	26.91/0.618	24.35/0.481	22.05/0.371	20.08/0.290	18.41/0.231
BM3D	37.13/0.943	33.62/0.883	31.86/0.839	30.72/0.804	29.85/0.775	29.16/0.750	28.56/0.728	27.99/0.707
OSC	37.79/0.964	33.66/0.888	31.97/0.817	30.60/0.758	29.68/0.712	29.00/0.689	28.46/0.661	27.98/0.653
				(16) Man 512 × 512				
B. Filter	31.40/0.843	30.93/0.836	29.38/0.765	26.91/0.626	24.31/0.485	21.99/0.376	20.02/0.298	18.37/0.241
BM3D	37.82/0.954	33.98/0.908	31.93/0.867	30.59/0.833	29.62/0.805	28.86/0.780	28.22/0.758	27.65/0.737
OSC	37.69/0.990	33.24/0.957	31.35/0.907	29.80/0.897	28.70/0.896	27.88/0.868	27.21/0.870	26.66/0.834

Table 3: PSNR/SSIM results for sixteen biomedical images.

Images	σ							
	5	10	15	20	25	30	35	40
Algae	39.37/0.898	36.66/0.818	35.61/0.776	34.47/0.741	33.50/0.703	32.68/0.660	32.01/0.620	31.49/0.586
c05c	39.31/0.944	36.11/0.876	34.71/0.822	33.43/0.790	32.43/0.760	31.60/0.734	30.93/0.714	30.38/0.697
celulas	38.19/0.978	34.40/0.926	32.88/0.880	31.62/0.835	30.72/0.802	30.01/0.771	29.41/0.755	28.91/0.726
crm04280	40.44/0.981	36.81/0.942	35.31/0.905	34.00/0.867	32.98/0.841	32.17/0.818	31.50/0.796	30.95/0.769
crm05210	39.49/0.984	35.36/0.940	33.48/0.904	31.98/0.871	30.85/0.845	30.01/0.822	29.30/0.800	28.74/0.776
cromo2	39.78/0.973	35.37/0.916	33.27/0.869	31.52/0.827	30.21/0.793	29.21/0.748	28.44/0.713	27.82/0.667
Fluocel	41.00/0.953	36.85/0.882	34.90/0.816	33.26/0.758	32.05/0.720	31.08/0.698	30.32/0.680	29.67/0.651
Heart	39.56/0.975	35.87/0.937	34.30/0.903	32.85/0.869	31.83/0.841	31.05/0.814	30.46/0.780	29.97/0.748
mr2	38.86/0.973	35.08/0.923	33.42/0.876	31.89/0.831	30.69/0.796	29.72/0.765	28.90/0.734	28.18/0.708
mr030	37.74/0.998	32.89/0.969	30.63/0.936	28.84/0.912	27.56/0.885	26.60/0.860	25.84/0.829	25.22/0.801
mr031	37.89/0.987	33.13/0.939	30.97/0.893	29.23/0.845	27.98/0.801	27.04/0.768	26.32/0.738	25.73/0.720
mr032	37.98/0.984	33.37/0.931	31.30/0.881	29.63/0.843	28.41/0.802	27.49/0.769	26.75/0.736	26.13/0.706
mr033	37.99/0.987	33.42/0.942	31.40/0.897	29.75/0.851	28.56/0.808	27.65/0.772	26.93/0.745	26.35/0.725
mr034	38.02/0.988	33.48/0.941	31.50/0.894	29.84/0.847	28.62/0.804	27.68/0.771	26.96/0.735	26.38/0.703
Muscle	38.02/0.966	33.55/0.905	31.48/0.851	29.71/0.807	28.40/0.768	27.41/0.738	26.60/0.723	25.91/0.698
X-ray	38.26/0.955	34.15/0.870	32.39/0.793	30.90/0.729	29.80/0.676	29.00/0.635	28.36/0.600	27.86/0.565

To validate the effectiveness, the proposed parameter optimization method is adapted to image denoising. In our experiments, a total of 256 noisy images were tested. They contained the noisy version of thirty-two noise-free images, corrupted by eight different levels of noise. Experimental results show that the proposed denoising method is effective in terms of the comparative results. The proposed method achieves better results than the Bilateral Filter; when the noisy standard deviation is less than 20, the proposed method slightly outperforms the BM3D method and is weaker than the BM3D method when the noisy standard deviation varies from 20 to 40.

Conflicts of Interest

The authors declare that there are no conflicts of interest regarding the publication of this paper.

Acknowledgments

This work was partially supported by National Natural Science Foundation of China under Grant no. 61300192, by Fundamental Research Funds for the Central Universities of China under Grant no. ZYGX2014J052, by Foundation Science and Forefront Technology of Chongqing Science &

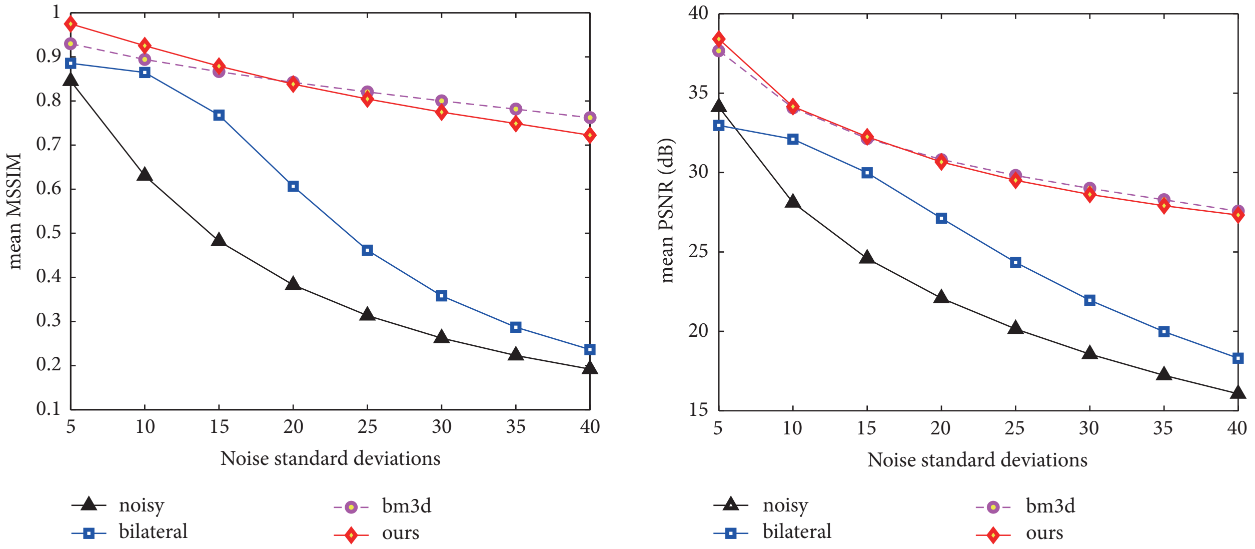

Figure 7: The mean PSNR and SSIM results for fixed noise from four methods.

Technology Commission under Grant no. cstc2016jcyjA0571, and by Ph.D. Cultivation Foundation of Chongqing University of Posts and Telecommunications under Grant no. RC 2016002.

References

[1] M. Ye, Y. Qian, and J. Zhou, "Multitask sparse nonnegative matrix factorization for joint spectral-spatial hyperspectral imagery denoising," *IEEE Transactions on Geoscience and Remote Sensing*, vol. 53, no. 5, pp. 2621–2639, 2015.

[2] Y. Peng, A. Ganesh, J. Wright, W. Xu, and Y. Ma, "RASL: robust alignment by sparse and low-rank decomposition for linearly correlated images," *IEEE Transactions on Pattern Analysis and Machine Intelligence*, vol. 34, no. 11, pp. 2233–2246, 2012.

[3] Y. Li, Y. Sun, and Y. Chi, "Low-rank positive semidefinite matrix recovery from corrupted rank-one measurements," *IEEE Transactions on Signal Processing*, vol. 65, no. 2, pp. 397–408, 2017.

[4] Y.-Q. Zhao and J. Yang, "Hyperspectral image denoising via sparse representation and low-rank constraint," *IEEE Transactions on Geoscience and Remote Sensing*, vol. 53, no. 1, pp. 296–308, 2015.

[5] B. Recht, M. Fazel, and P. A. Parrilo, "Guaranteed minimum-rank solutions of linear matrix equations via nuclear norm minimization," *SIAM Review*, vol. 52, no. 3, pp. 471–501, 2010.

[6] J.-F. Cai, E. J. Candes, and Z. Shen, "A singular value thresholding algorithm for matrix completion," *SIAM Journal on Optimization*, vol. 20, no. 4, pp. 1956–1982, 2010.

[7] S. Gu, L. Zhang, W. Zuo, and X. Feng, "Weighted nuclear norm minimization with application to image denoising," in *Proceedings of the 27th IEEE Conference on Computer Vision and Pattern Recognition (CVPR '14)*, pp. 2862–2869, June 2014.

[8] G. Gasso, A. Rakotomamonjy, and S. Canu, "Recovering sparse signals with a certain family of nonconvex penalties and DC programming," *IEEE Transactions on Signal Processing*, vol. 57, no. 12, pp. 4686–4698, 2009.

[9] C. Lu, J. Tang, S. Yan, and Z. Lin, "Generalized nonconvex nonsmooth low-rank minimization," in *Proceedings of the 27th IEEE Conference on Computer Vision and Pattern Recognition (CVPR '14)*, pp. 4130–4137, June 2014.

[10] Y. Hu, D. Zhang, J. Ye, X. Li, and X. He, "Fast and accurate matrix completion via truncated nuclear norm regularization," *IEEE Transactions on Pattern Analysis and Machine Intelligence*, vol. 35, no. 9, pp. 2117–2130, 2013.

[11] J. Yang, Y.-Q. Zhao, J. C.-W. Chan, and S. G. Kong, "Coupled sparse denoising and unmixing with low-rank constraint for hyperspectral image," *IEEE Transactions on Geoscience and Remote Sensing*, vol. 54, no. 3, pp. 1818–1833, 2016.

[12] Y. Wang and X. Su, "Truncated nuclear norm minimization for image restoration based on iterative support detection," *Mathematical Problems in Engineering*, vol. 2014, Article ID 937560, 2014.

[13] F. G. Meyer and X. Shen, "Perturbation of the eigenvectors of the graph Laplacian: application to image denoising," *Applied and Computational Harmonic Analysis*, vol. 36, no. 2, pp. 326–334, 2014.

[14] S. Gu, Q. Xie, D. Meng, W. Zuo, X. Feng, and L. Zhang, "Weighted nuclear norm minimization and its applications to low level vision," *International Journal of Computer Vision*, vol. 121, no. 2, pp. 183–208, 2017.

[15] N. El Karoui, "On information plus noise kernel random matrices," *The Annals of Statistics*, vol. 38, no. 5, pp. 3191–3216, 2010.

[16] C. Tomasi and R. Manduchi, "Bilateral filtering for gray and color images," in *Proceedings of the IEEE 6th International Conference on Computer Vision*, pp. 839–846, January 1998.

[17] K. Dabov, A. Foi, V. Katkovnik, and K. Egiazarian, "Image denoising by sparse 3-D transform-domain collaborative filtering," *IEEE Transactions on Image Processing*, vol. 16, no. 8, pp. 2080–2095, 2007.

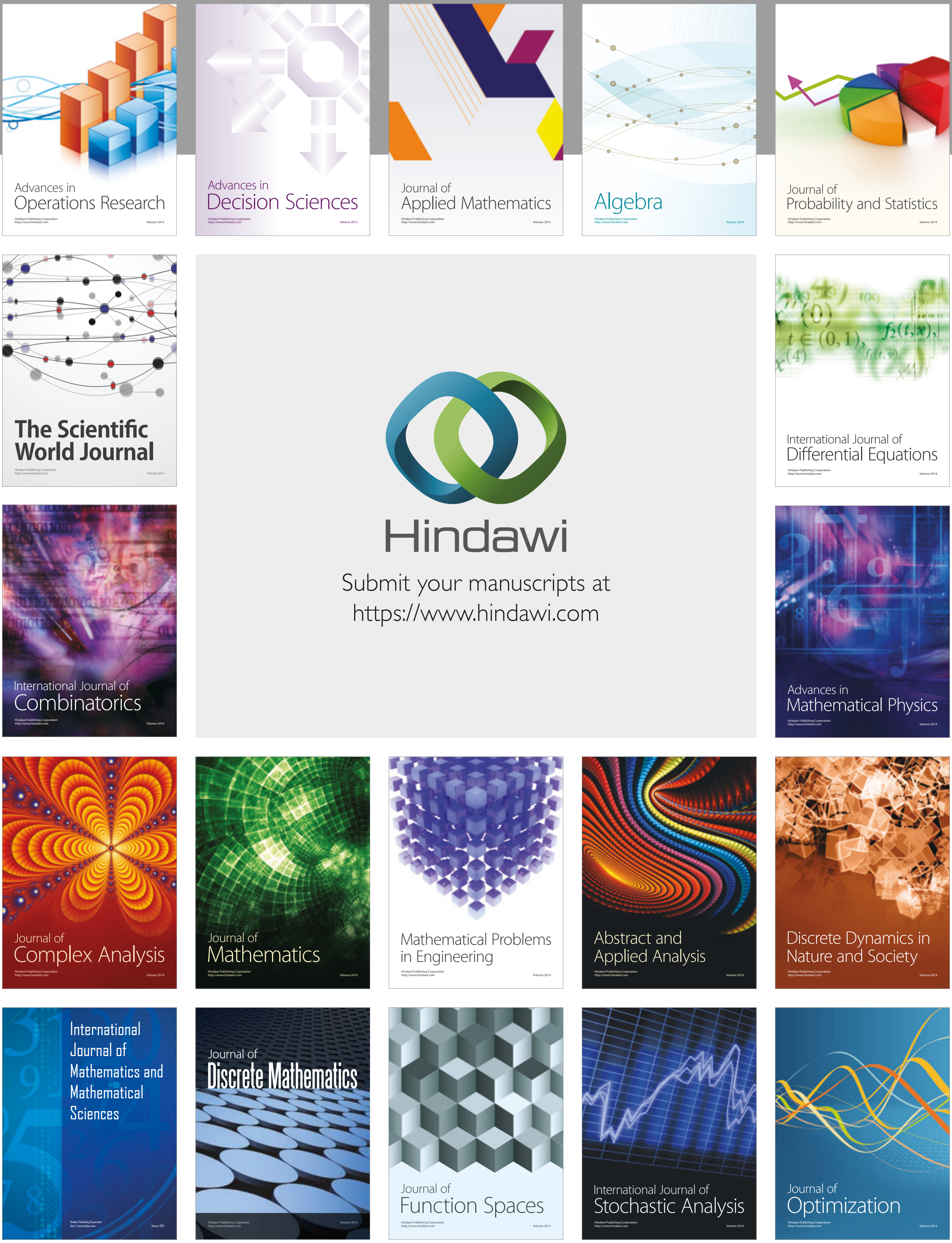
Advances in Operations Research
Advances in Decision Sciences
Journal of Applied Mathematics
Algebra
Journal of Probability and Statistics
The Scientific World Journal
International Journal of Differential Equations
International Journal of Combinatorics
Advances in Mathematical Physics
Journal of Complex Analysis
Journal of Mathematics
Mathematical Problems in Engineering
Abstract and Applied Analysis
Discrete Dynamics in Nature and Society
International Journal of Mathematics and Mathematical Sciences
Journal of Discrete Mathematics
Journal of Function Spaces
International Journal of Stochastic Analysis
Journal of Optimization

Hindawi

Submit your manuscripts at
https://www.hindawi.com